Conjugation of a peptide autoantigen to gold nanoparticles for intradermally administered antigen specific immunotherapy

Dul M[1,*], Nikolic T[2,*], Stefanidou M[1], McAteer MA[4], Williams P[4], Mous J[4], Roep BO[2,3], Kochba E[5], Levin Y[5], Peakman M[6], Wong FS[7], Dayan CM[7], Tatovic D[7,0], Coulman SA[1,+], Birchall JC[1,+] on behalf of the EE-ASI Consortium

[1]School of Pharmacy and Pharmaceutical Sciences, Cardiff University, UK
[2]Leiden University Medical Centre, Leiden, The Netherlands
[3]Beckman Research Institute at the City of Hope, Duarte, CA, USA
[4]Midatech Pharma plc, Abingdon, UK
[5]NanoPass Technologies Ltd., Nes Ziona, Israel.
[6]Dept of Immunobiology, King's College London, UK
[7]Diabetes Research Group, School of Medicine, Cardiff University, UK

[*]These authors contributed equally to this work
[+]Joint Senior Authors
[0]To whom correspondence should be addressed

Address for correspondence:
Dr Danijela Tatovic
Diabetes Research Group
Division of Infection and Immunity
Cardiff University School of Medicine
Heath Park
Cardiff CF14 4XN, UK
Tel:(+44) 078 333 23 677
E-mail: tatovicd@cardiff.ac.uk

ABSTRACT

Antigen specific immunotherapy aims to tolerise patients to specific autoantigens that are responsible for the pathology of an autoimmune disease. Immune tolerance is generated in conditions where the immune response is supressed and thus gold nanoparticles (AuNPs) are an attractive drug delivery platform due to their anti-inflammatory effects and their potential to facilitate temporal and spatial delivery of a peptide autoantigen in conjunction with pro-tolerogenic elements. In this study we have covalently attached an autoantigen, currently under clinical evaluation for the treatment of type 1 diabetes ($PI_{C19\text{-}A3}$ peptide), to AuNPs to create nanoscale (<5nm), negatively charged (-40 to -60mV) AuNP-peptide complexes for immunotherapy. We also employ a clinically approved microneedle delivery system, MicronJet600, to facilitate minimally-invasive intradermal delivery of the nanoparticle constructs to target skin-resident antigen presenting cells, which are known to be apposite target cells for immunotherapy. The AuNP-peptide complexes remain physically stable upon extrusion through microneedles and when delivered into *ex vivo* human skin they are able to diffuse rapidly and widely throughout the dermis (their site of deposition) and, perhaps more surprisingly, the overlying epidermal layer. Intracellular uptake was extensive, with Langerhans cells proving to be the most efficient cells at internalising the AuNP-peptide complex (94% of the local population within the treated region of skin). In vitro studies showed that uptake of the AuNP-peptide complexes by dendritic cells reduced the capacity of these cells to activate naïve T cells. This indicator of biological functionality encourages further development of the AuNP-peptide formulation, which is now being evaluated in clinical trials.

Keywords: gold nanoparticles, peptide, antigen specific immunotherapy, microneedles, diabetes

1. INTRODUCTION

Antigen specific immunotherapy (ASI) uses autoantigen molecules or peptide epitopes thereof to promote immune tolerance in individuals with antigen specific autoimmune conditions e.g. Type 1 diabetes (T1D). This therapeutic approach attempts to address the immunological aetiology of an autoimmune disease rather than provide replacement treatment and this has a raft of potential clinical benefits. However, there is a delicate balance between homeostatic immune tolerance mechanisms to self-peptide and the inflammatory immune response to a foreign antigen. Moderation of this balance *in vivo* is a significant challenge and whilst ASI has been successful in animal models, translation to humans has proved challenging(von Herrath et al., 2013). Selection of the peptide autoantigen, its formulation and the route of delivery are all recognised as key parameters that need to be better understood and optimised to facilitate future clinical success (Hirsch and Ponda, 2015).

In this study we selected the HLA-DR4 (DRB1*0401) restricted proinsulin peptide $PI_{C19\text{-}A3}$ as a potential immunomodulatory treatment to delay, or even prevent, the onset of T1D. This peptide is associated with positive safety data in phase 1 clinical trials and is thought to function by modulating autoreactive CD4 T-cells (Thrower et al., 2009), thus preserving beta-cell function (Alhadj Ali et al., 2017). Our ambition is to use this peptide in conjunction with an immunomodulating element that could induce a local tolerogenic environment that directs the immune response towards regulation rather than inflammation. However, to achieve this ambition a drug delivery platform is required that can facilitate concomitant delivery of multiple therapeutic cargos and control the localised kinetics to ensure an appropriate bystander effect. This study has therefore used ultra-small (5nm) carbohydrate-coated gold nanoparticles (AuNPs) with a high surface area-to-volume ratio (thus making them particularly suitable for the dense loading of therapeutic cargos (Love et al., 2005)), a multi-valent surface structure (for covalent or non-covalent conjugation to the surface (Ghosh et al., 2008; Kim et al., 2010; Rana et al., 2012)) and a tightly controlled dispersity to provide a platform for $PI_{C19\text{-}A3}$ delivery. In tolerogenic approaches the aim is to minimise immune stimulation and promote a

regulatory response and therefore we hypothesise that exploiting a AuNP platform with known anti-inflammatory properties (de Araujo et al., 2017) and clinical potential (Rana et al., 2012) may also be beneficial.

Whilst AuNPs may provide an appropriate multi cargo delivery platform, it is also important to consider how to target this delivery vehicle to the target cells. The skin is rich in antigen presenting cells (APCs) and therefore has been extensively exploited as a dose-sparing route for conventional vaccination (Henri et al., 2010; Merad et al., 2008). However the APCs in this organ, the dendritic cells (DCs) and particularly Langerhans Cells (LCs), also have pivotal roles in immune regulation and tolerance (Mutyambizi et al., 2009). Whilst delivery of our AuNP peptide construct to the skin could take advantage of the immune regulatory functions of these APCs, it will be important to minimise the inflammation that is caused when the outermost skin barrier, the stratum corneum, is breached. Microneedles (MNs) therefore provide an appropriate means of delivery. MNs are ultra-short needles that have previously been used for dose-sparing intradermal vaccinations (Coulman et al., 2006; Edens et al., 2015a; Edens et al., 2015b; Pearton et al., 2013), causing minimal tissue disruption and no pain or bleeding upon clinical use. Recent studies have also started using these devices for intradermal administration of a tolerogenic auto-antigen, leading to effective presentation of antigen to T cells in skin draining lymph nodes and reduced antigen-specific T cell proliferation in the pancreatic lymph node (Zhao et al., 2016). However, there are many types of MNs and each has different advantages and disadvantages, depending on their form and function (Prausnitz, 2017). Previous studies have dry coated a naked peptide auto-antigen onto stainless steel MNs prior to their intradermal administration (Zhao et al., 2016). However, the deposition and local kinetics of the coated formulation are predominantly dictated by the nature of the biological environment and the physicochemical properties of the therapeutic, i.e. dissolution of the peptide in the biological milieu. As an alternative, hollow MNs provide a clinically approved (Beals et al., 2016; Bragazzi et al., 2016) system that uses either single needles or a plurality of microstructures for delivery of a discrete volume of a liquid formulation into the intradermal space. The MicronJet600

device, from NanoPass Technologies Ltd, is a hollow CE-marked MN device for clinical use and has stimulated robust immune responses to vaccines (Levin et al., 2015) at potentially reduced antigen doses. The sterile device is mounted on a standard syringe in much the same way as a conventional hypodermic needle, allowing for simple and reliable use and disposal. It has therefore been adopted in this study to provide a reproducible minimally invasive conduit into the skin for the AuNP self-antigen delivery platform.

This study describes the pre-clinical investigations that have characterised the physicochemical properties of the $PI_{C19\text{-}A3}$ conjugated AuNPs, their physical stability upon extrusion through MicronJet600 MNs, the distribution of $PI_{C19\text{-}A3}$ AuNPs within *ex vivo* human skin after MN injection, the uptake of $PI_{C19\text{-}A3}$ AuNPs by human skin cells and the effect of this uptake on DCs. These studies have been crucial to provide our consortium, The Enhanced Epidermal Antigen Specific Immunotherapy Against Type 1 Diabetes (EE-ASI) consortium (www.ee-asi.eu), with the understanding needed to translate the AuNP platform to the clinic for the immune intervention therapy of Type 1 diabetes.

2. MATERIAL AND METHODS

All reagents and laboratory consumables were purchased from Fisher Scientific, UK unless otherwise indicated. Proinsulin peptide $PI_{C19\text{-}A3}$ (AmbioPharm Inc, North Augusta, SC, USA) and $GAD_{339\text{-}352}$ peptide (Innovagen AB, Sweden) were synthesised with a thiol linker to enable covalent binding to AuNPs.

2.1. Microneedle devices

The MN device used in this study (MicronJet600 (MJ600); NanoPass Technologies Ltd) consists of 3 pyramid-shaped MNs of 0.6 mm (600 μm) length integrated with a plastic hub that can be attached to any standard Luer syringe (Supplementary Figure 1).

2.2. AuNP characterization

AuNPs were synthesized and supplied by Midatech Pharma. Peptide loaded AuNPs were manufactured containing three peptide concentrations (3%, 5% and 10%) and either a glucose or mannose carbohydrate moiety. The identities of the formulations used in specific elements of the work are detailed in the relevant results and figure legends. Morphological analysis was performed by transmission electron microscopy (TEM; JEM-2100 LaB6, JEOL, USA). Samples were applied to a grid and dried for approximately 60 s under ambient conditions. Mean particle size (hydrodynamic particle size) was determined by dynamic light scattering (DLS) using 173° backscatter detection. Electrophoretic mobility was measured by Laser Doppler Velocimetry (LDV) and converted to zeta potential (ZP) values using the Smoluchowski equation. Both measurements (DLS and LDV) were performed on formulations in triplicate, both before and after MN injection, using a Zetasizer Nano ZS series Nano-ZS ZEN3600 fitted with a 633 nm laser (Malvern Instruments Ltd., UK). Changes to gold concentration following MN injection was assessed by UV/vis absorption at 405 nm using a BMG FLUOstar Optima microplate reader.

2.3. Collection, processing and maintenance of *ex vivo* human skin

Human skin samples were obtained from female patients aged 38-86 years, following mastectomy or breast reduction under informed patient consent and ethical approval (South East Wales Local Research Ethics Committee; 08/WSE03/55). Excised skin was collected immediately after surgery and transported at 4°C in media consisting Dulbecco's modified Eagle medium (DMEM; Life Technologies, UK), 100 unit ml^{-1} penicillin and 100 µg ml^{-1} streptomycin (ThermoFisher Scientific Ltd, UK). Subcutaneous adipose tissue was removed by blunt dissection and skin was pinned, dermis side down, onto a cork dissection board to facilitate MN injection.

2.4. Visualising AuNP distribution within skin sections by microscopy

AuNPs (blank and conjugated to $PI_{C19\text{-}A3}$) and commercially available 50nm colloidal AuNPs (Sigma-Aldrich, UK) were injected (50 µl in PBS) into *ex vivo* human skin via MJ600 MNs. Following injection, 8 mm biopsy punches were extracted and placed into fixative (4% v/v formaldehyde / 0.2% glutaraldehyde, pH 7.3; t = 0 h) or incubated for 4 h at air-liquid interface at 37 °C in an atmosphere of 5% (v/v) CO_2/95% (v/v) air before fixation. Processing for transmission electron (TEM) or light microscopy involved bisection along the injection site, post-fixation in either 2% aqueous uranyl acetate or 0.2% (w/v) aqueous osmium tetroxide, washing in water, dehydration through graded propan-2-ol and embedding in LR White acrylic resin (London Resin Company, Reading, U.K.). The resulting resin-embedded sample was mounted in an ultramicrotome and the block face trimmed to a trapezium with a glass knife. For light microscopy, 0.4 µm sections were collected onto Vectabond-treated glass slides (Vector Labs, Peterborough, UK) and dried at 50°C. For visualization of AuNPs, sections of uranyl-acetate post-fixed tissue were incubated directly in Newman and Jasani's physical developer (Newman and Jasani, 1998). Sections of osmium tetroxide post-fixed samples were additionally pre-treated for 1 h with saturated sodium periodate before incubation in the physical developer. Prepared slides were counterstained with Goldner's Light Green (0.2% w/v Light Green SF in 0.2% v/v acetic acid) and visualized with an Olympus BX 51 research light microscope fitted with a Zeiss

Axiocam digital camera. For TEM, 100 nm sections were collected onto EM grids, stained with uranyl acetate and lead citrate, and examined in the CM12 TEM (FEI (UK Ltd), UK).

2.5. Human cells

2.5.1. HaCaT cell culture. Immortalized human keratinocyte cells, HaCaT cells(Boukamp et al., 1988), were received as a gift from Professor Mark Gumbleton (School of Pharmacy and Pharmaceutical Sciences, Cardiff University). Cells were cultured in growth medium (DMEM supplemented with 10% v/v fetal bovine serum (FBS; VWR International, UK), 100 unit ml^{-1} penicillin and 100 µg ml^{-1} streptomycin) at 37°C in a humidified atmosphere containing 5% v/v CO_2.

2.5.2. Isolation and culture of primary keratinocytes. A superficial layer of the skin (collected and prepared as described in section 2.3) was separated using a surgical blade and transferred into a centrifuge tube containing 0.25% (w/v) trypsin solution and stored overnight at 4°C. Suspended cells were filtered through a 70 µm cell strainer and centrifuged at 300 x *g* for 7 min. The cell pellet was gently re-suspended in media containing EpiLife medium (Life Technologies, UK) supplemented with 10% human keratinocyte growth supplement (Life Technologies, UK), 100 unit ml^{-1} penicillin, 100 µg ml^{-1} streptomycin and 2.5 µg ml^{-1} amphotericin B (VWR International, UK) and seeded in a 25 cm^3 flask. The media was changed every 2-3 days until primary cells reached 70-80% confluency.

2.5.3. Fresh isolation of human skin cell suspensions. After collection and preparation of the skin sample as described in section 2.3 the bulk of lower dermis was removed by blunt dissection. The remaining tissue containing epidermis and upper dermis was cut into small pieces and immersed in enzyme cocktail solution containing Dispase II (2 units ml^{-1}), Collagenase I (197 units ml^{-1}) and Deoxyribonuclease I (DNA-se I) from bovine pancreas (20 units ml^{-1}) in Roswell Park Memorial Institute (RPMI) 1640 media (Sigma-Aldrich, UK) for 1 h at 37°C.

Following incubation, epidermal sheets were mechanically separated and transferred into 0.25% (w/v) trypsin solution in PBS for 30 min at 37°C (Boyce and Ham, 1983). After incubation, soybean trypsin inhibitor (1 mg ml^{-1}) was added and the epidermal cell suspension was filtered through a 70 μm cell strainer, centrifuged at 400 x g for 10 min and re-suspended in the appropriate solution depending on the experimental procedure. Dermal cells were isolated using a 'walkout' protocol. Separated dermis was placed in RPMI media supplemented with 10% (w/v) human AB serum, 100 unit ml^{-1} penicillin, 100 μg ml^{-1} streptomycin and 2.5 μg ml^{-1} amphotericin B and incubated at 37°C for 48 h. Dermal cells present in the media were filtered through a 70 μm cell strainer, centrifuged at 400 x g for 10 min and re-suspended in the appropriate solution depending on the experimental procedure.

2.5.4. *In vitro* generation of human dendritic cells (DCs). Monocyte-derived dendritic cells (moDC) were generated as previously described (Kleijwegt et al., 2010). In short, peripheral blood mononuclear cells (PBMCs) were isolated from buffy coats of healthy donors and monocytes were purified by CD14-specific positive magnetic cell sorting according to the supplier's protocol (MACS, Miltenyi Biotec, Germany). Isolated monocytes (~90% pure) were cultured in RPMI 1640 medium supplemented with antibiotics and 10% heat-inactivated fetal calf serum (FCS, Greiner, Wemmel, Belgium). DC differentiation was induced using recombinant human IL-4 (500 U ml^{-1}, Invitrogen, The Netherlands) and recombinant human GM-CSF (800 U ml^{-1}, Invitrogen). Medium and cytokines were refreshed on day 3. On day 6, immature moDCs were harvested and cryopreserved until subsequent stimulation.

2.6. Cellular uptake of FITC-labelled AUNPs

AuNPs were conjugated to a FITC-labelled peptide and this construct was used to determine cell uptake. The small distance between conjugated FITC-labelled peptide molecules and the gold quenches the fluorescence (Loumaigne et al., 2010). However, once the peptide is cleaved from the AuNP the FITC fluorescence

can be detected by fluorescent microscopy or flow-cytometry. This occurs intracellularly and therefore is a marker of cellular uptake and cleavage/processing.

2.6.1. Cellular uptake of FITC-labelled AuNPs in human keratinocyte cell lines. Twenty-four hours before treatment, HaCaT (passage 77-86) or primary keratinocyte (passage 6-10) cells were seeded into 24-well plates at a density of $1x10^5$ per well in 0.5 ml of growth medium. Cell populations were then washed with PBS and treated with 0.5 ml of various FITC-labelled AuNP formulations at 10 μg ml^{-1} (with respect to gold concentration) in serum-free media (DMEM, 100 unit ml^{-1} penicillin and 100 μg ml^{-1} streptomycin). Serum-free media was used as a control. Following 30 min, 4 h, 24 h, 48 h or 72 h incubation AuNPs were removed, cells were washed twice with PBS and trypsinised at 37°C for 10 min with trypsin-EDTA. Cells were then re-suspended in growth medium, centrifuged at 300 × *g* for 5 min and washed with PBS. Pelleted cells were fixed with 100 μL fixation buffer (BD Biosciences, UK) for 15 min at 4°C, washed and re-suspended in 200 μl of stain buffer (BSA), (BD Biosciences, UK) before flow cytometry analysis (FACSVerse™, BD Biosciences, UK) using a 3-laser, 8-color (4-2-2) configuration.

For confocal microscopy HaCaT or primary keratinocyte cells were seeded in glass bottom dishes (MatTek Corporation, USA) at a density of $3x10^5$ per well in 1.5 ml of growth media. Cell populations were then washed with PBS and treated with 1.5 ml of various types of AuNPs prepared at concentration of 10 μg ml^{-1} (with respect to gold) in serum-free media. Serum-free media was used as a control. Following 30 min, 4 h and 24 h of incubation the nanoparticle suspension was removed from the cell surface and cells were washed twice with PBS before the addition of EpiLife imaging media to conduct imaging studies using a DMI 6000 Leica confocal microscope equipped with 350, blue diode 405, Argon 488 and HeNe 543 and 633nm lasers.

2.6.2. Cellular uptake of FITC-labelled AuNPs in mixed cell suspensions from human skin. Mixed cell suspensions of epidermal/dermal cells were isolated as described in section 2.5.3. Cells were further counted and placed in 96-well round bottom plate (Corning Costar, UK) at cell densities of $1x10^5$ per well in 100 µl of RPMI serum-free media. Fluorescently labelled AuNPs were prepared in RPMI serum-free media at 20 µg ml^{-1} (with respect to gold) and 100 µl of prepared formulation were added to each well (final AuNP concentration 10 µg ml^{-1}). Following incubation at 37°C in a humidified atmosphere containing 5% v/v CO_2, the cells were pelleted by centrifugation at 400 × *g* for 10 min and washed with PBS. Pelleted cells were fixed with 100 µl fixation buffer for 15 min at 4 °C, washed and re-suspended in 200 µl stain buffer (BSA), (BD Biosciences, UK) before flow cytometry analysis.

For confocal microscopy a single cell suspension of epidermal/dermal cells was exposed to fluorescently labelled AuNPs as described in section 2.6.1. Following incubation with AuNPs, cells were washed in PBS, pelleted by centrifugation at 400 × *g* for 10 min, re-suspended in 100 µL of EpiLife media and placed in glass bottom dishes for live cell imaging.

2.6.3. Extracting cells from excised human skin, previously injected with FITC-labelled AuNPs, to determine cellular uptake *ex vivo*. Fresh human skin was obtained and processed as described in section 2.5.3. Following tissue preparation, the skin was pinned, dermis side down, onto a cork dissection board and 50 µl of FITC-labelled AuNPs or PBS (as control) were injected using the MJ600 device. Thereafter 8 mm biopsy punches were incubated for 4 or 24 h at the air-liquid interface at 37°C and 5% v/v CO_2. Injections were performed in at least triplicate. Biopsy punches were subsequently processed by enzymatic separation of epidermis from dermis as described in the section 2.5.3. Isolated skin cells were washed in PBS and prepared for either flow cytometry or confocal microscopy as described in the previous section.

2.6.4. Immunostaining cells extracted from excised human skin injected with FITC-labelled AuNPs. Single cell suspensions from untreated and treated (FITC-labelled $PI_{C19\text{-}A3}$ AuNP) skin explants were prepared as described in the section 2.5.3. The cells were centrifuged at 400 × *g* for 10 min and re-suspended in the relevant antibodies in stain buffer (BSA), (BD Biosciences, UK). Epidermal cells were stained with V450 mouse anti-human HLA-DR (dilution 1:50, BD Biosciences, UK) and PE anti-human CD207 (dilution 1:50, BioLegend, UK), while dermal cells were stained with V450 mouse anti-human HLA-DR (dilution 1:50, BD Biosciences, UK) and CD11c human APC (dilution 1:20, Miltenyi Biotec Ltd., UK). Mixtures were incubated for 1 h in the dark at 4°C and the staining process used a 100 µl staining media with $1x10^5$ cells/test. Simultaneously, for compensation purposes, the appropriate species matching compensation beads (Anti-Mouse Ig, **κ**/Negative Control Compensation Particles Set, BD Biosciences, UK) were incubated separately with each dye under the same conditions. After incubation, cells were centrifuged at 400 x g, washed and re-suspended in 200 µl of stain buffer (BSA) before flow cytometry. Filters that were used include SSC (488/15), FITC (527/32), PE (586/42), APC (660/10) and V450 (448/45).

2.6.5. Cellular uptake of FITC-labelled AuNPs in human moDCs. Immature DCs were incubated with FITC-labelled AuNPs for 4 h to allow uptake, after which free AuNPs were washed away by centrifugation. The DCs were subsequently cultured overnight in standard growth medium or 100 ng ml^{-1} LPS (Sigma Aldrich Chemie, The Netherlands) where indicated. Staining of moDCs was analysed by flow cytometry (FACS Calibur™, BD Biosciences, UK).

2.7. *In vitro* T cell stimulation by human moDCs treated with FITC-labelled AuNPs

T cell stimulatory capacity of control or AuNP-treated DCs was tested using either an effector T cell clone specific for GAD65 peptide ($GAD_{339\text{-}352}$)(Schloot et al., 1999) or allogeneic $CD4^+$ T cells, which were isolated from PBMCs using a negative selection kit (Dynal, Invitrogen, The Netherlands). $CD4^+$ T cells were

plated at 10^5 T cells per well with different ratios of DCs and cultured in IMDM (Dulbecco) supplemented with 10% human serum. Four days later, cell cultures were pulsed overnight with [^{3}H]-thymidine and incorporation was determined.

2.8. Data processing

Flow cytometry data were analysed using FlowJo Flow Cytometry Analysis Software for Mac Version 10.0 (Tree Star Inc., USA). Image processing including scale bar inclusion was performed using ImageJ software (National Institute of Health, USA).

3. RESULTS AND DISCUSSION

The intradermal delivery of an auto-antigen loaded AuNP using a minimally invasive MN delivery system to enhance autoantigen uptake into, and promote tolerance from, relevant APCs combines technologies and knowledge from the pharmaceutical sciences and immunology to provide a potential treatment for the improvement of antigen-specific immunotherapy for T1D. Development, characterisation and incremental optimisation of the system is fundamental to clinical translation and success.

Initial studies ensured that AuNP-peptide complexes could be manufactured and tuned to ensure physical stability upon extrusion through MNs. AuNPs used in this study comprise a core of gold atoms to which an organic layer of carbohydrates (glucose (G) or mannose (M)), glutathione (GSH) and proinsulin peptide ($PI_{C19\text{-}A3}$) were attached, via sulphur bonds (Figure 1A). GSH enables non-enzymatic intracellular activation / release of prodrugs (Sies, 1999), based on the difference in intracellular GSH concentration (1-10 mM) relative to extracellular thiol levels (2 μM glutathione, 8 μM cysteine) (Jones et al., 1998) and provides a negative surface charge that could potentially be used for electrostatic loading of further elements. The carbohydrate moiety was included to enhance solubility of the constructs and has previously been shown to heighten uptake of NPs (Kang et al., 2015; Rana et al., 2012), including gold nanoclusters (<3nm) (Fernandez et al.,

2015), by monocyte derived DCs (MoDCs). The amount of each ligand utilised in the AuNP corona synthesis reaction is expressed in terms of relative percentage by weight, for example AuNP synthesised with 3% peptide and 5% glucose would also contain 92% GSH by weight. Transmission electron microscopy (TEM) indicated that suspensions of the AuNP-peptide complexes were relatively homogenous with a nanoparticle diameter of 2-4nm, irrespective of the peptide concentration (1%, 3% and 10%) or sugar moiety used in the formulation (G or M) (Figure 1B-D). Dynamic laser scattering data generally supported TEM observations and, importantly, injection through MicronJet600 MNs (MJ600) did not change the diameter of AuNPs (Figure 1E). UV/Vis absorbance measurements confirmed no loss of AuNPs following their injection through MJ600 MNs (Figure 1F) and complexes containing both 1% and 3% peptide remained negatively charged (-40mV to -60mV) following their extrusion through the micron-sized MN bore (Figure 1E). These data sets indicate that the AuNP colloidal formulation is physically stable to the shear forces that are created upon injection and does not irreversibly interact with the MJ600 materials. However, the zeta potential distribution profiles of AuNPs formulated with 10% peptide were notably altered following MN extrusion (Supplementary Figure 2), which indicates physical instability of the formulation at the higher $PI_{C19\text{-}A3}$ doses and a maximum loading capacity of 5-10% for the selected AuNPs. Subsequent studies therefore adopted a AuNP formulation containing 3% peptide and the volume of formulation was tailored to achieve the anticipated therapeutic dose (10μg) of $PI_{C19\text{-}A3}$ (Thrower et al., 2009).

In order to promote a regulatory response to the $PI_{C19\text{-}A3}$ autoantigen we employed the CE-marked MJ600 device to target skin DCs whilst minimising the trauma of intradermal delivery and any ensuing cutaneous inflammation (Mutyambizi et al., 2009). The device has three hollow silicon MNs of 600μm length and has been used extensively in clinical studies to deliver a range of macromolecular formulations including insulin (Kochba et al., 2016), varicella zoster (Beals et al., 2016), polio (Anand et al., 2015; Troy et al., 2015) and seasonal and pandemic

influenza vaccines (Della Cioppa et al., 2014; Hung et al., 2012a; Hung et al., 2012b; Levin et al., 2014; Levin et al., 2016; Van Damme et al., 2009). However, whilst there are a number of publications showing successful therapeutic readouts upon use of hollow MNs, there is a paucity of information related to the behaviour of injected materials in the local environment and how formulation or physicochemical drug properties influence distribution and retention *in situ* (Mansoor et al., 2015). Local kinetics and the interactions of the $PI_{C19\text{-}A3}$ AuNP construct with the cellular and extracellular environment in the skin will be key to the potential therapeutic effects. A silver staining technique was therefore used to visualise tissue distribution of AuNPs (initially placebo AuNPs without auto-antigen) in the skin following MJ600 MN injection. AuNPs were detectable in both the viable epidermis (Figure 2B, C) and the dermis. Repeat studies using AuNP complexes covalently linked to $PI_{C19\text{-}A3}$ supported these initial observations, illustrating that after just four hours the $PI_{C19\text{-}A3}$ AuNP complex had diffused extensively from the injection site throughout the papillary and reticular dermis, with accumulation at the basement membrane zone and in cells of the viable epidermis (Figure 2E). These results contrasted with parallel studies that used larger colloidal AuNPs (50 nm diameter) as control (Figure 2F) and previously published studies using polystyrene NPs (50-100nm diameter) (Coulman et al., 2009; McAllister et al., 2003), whereby MN delivered NPs were retained in the dermis in close association with collagen and elastin fibres. Within the intradermal space the ultra-small AuNPs therefore behave more like a solution than the more conventional colloidal formulation of larger NPs (Labouta et al., 2011). Their greater diffusive properties (Fernandez et al., 2015; Kohli and Alpar, 2004; Sonavane et al., 2008) enable the AuNP-peptide complex to reflux from the point of dermal deposition, across the tightly packed basement membrane and into the viable epidermis of human skin. This is potentially advantageous as the epidermis is the most cellular region of the tissue and contains a vast network of epidermal Langerhans cells, which are key mediators in tolerisation mechanisms (Deckers et al., 2018).

TEM enabled closer scrutiny of the distribution of $PI_{C19\text{-}A3}$ loaded AuNPs in human skin at the cellular level. Following MJ600 delivery AuNPs were co-localised within cells that had phenotypic characteristics indicative of keratinocytes (Figure 3A), epidermal dendritic cells, i.e. LCs with signature Birbeck granules (Figure 3B) and dermal cells (Figure 3C). These observations were supported by *in vitro* studies in immortalised keratinocytes, primary keratinocytes and freshly isolated human skin cells, all of which demonstrated efficient uptake of FITC-labelled $PI_{C19\text{-}A3}$ AuNPs following topical application (Supplementary Video 1; Supplementary Figure 3). Whilst cultured cell lines (HaCaT cells and primary keratinocytes) required a contact time between 30min and 4 h for cell uptake, cells that were freshly extracted from human skin were able to internalise the AuNP complex after a contact time of just 30 min (Supplementary Figure 3a). This indicates that a delivery method which is able to facilitate direct contact between skin cells and the AuNP complex *in vivo,* is likely to facilitate rapid cell uptake.

Studies progressed to further examine and quantify cell uptake of the AuNPs *in situ*. Following MJ600 delivery of $PI_{C19\text{-}A3}$ AuNPs into freshly excised human skin tissue, cells were subsequently extracted and analysed by flow cytometry. Immunostaining of these cells identified HLA-DR+/CD207+ (epidermal LCs) (Figure 4A) and HLA-DR+/CD11c+ (dermal DCs) (Figure 4B) cells within the total extracted epidermal and dermal cell populations respectively. After 4 h, 94% of the extracted LCs and 29% of the dermal DCs were FITC positive, compared to 34% and 46% of the other epidermal and dermal cells respectively (Figure 4C). Confocal microscopy confirms that the $PI_{C19\text{-}A3}$ AuNPs associated with these cells are internalised, rather than binding to the exterior of the cell membrane, with AuNPs visualised throughout the cell cytoplasm (Figure 5, Supplementary Video 1).

This data indicates preferential internalisation of the $PI_{C19\text{-}A3}$ AuNP complex by epidermal LCs *in situ*. Whilst the differences in the isolation techniques for the epidermal and dermal cells may contribute to this disparity between LCs and dermal DCs (dermal DCs are isolated from skin using a walk out method, whereas

LCs are isolated by enzymatic digestion of the epidermis), *in vitro* data (Supplementary Figure 3) also indicates that epidermal cells internalise the AuNP complex more efficiently than dermal cells. This supports the notion of preferential uptake of the AuNP construct by epidermal LCs. Enhanced uptake may be attributed to a greater contact area between the formulation and LCs as a result of their extensive network of dendrites that probe across multiple cellular layers of the viable epidermis, the mobility of LCs within the excised human tissue, the greater propensity of these APCs to internalise foreign materials or a combination of these factors (Deckers et al., 2018).

LCs are constantly sampling the local environment and migrating to lymph nodes to present antigens. In the non-activated state, LCs present self-antigens and this is thought to be key to tolerance mechanisms and homeostasis. However, upon injury, infection or inflammation LCs are stimulated to help orchestrate a pathogenic immune response. Therefore whilst successful delivery of the $PI_{C19\text{-}A3}$ AuNPs to the relevant APCs is a key pre-cursor to our tolerogenic strategy, it must be followed by cellular presentation of the peptide to naïve T cells that subsequently adopt a regulatory rather than inflammatory phenotype (Banchereau and Steinman, 1998). moDCs provide an APC laboratory model that whilst not identical to those LCs found in skin, can be used to probe biological effects due to their comparable phenotype and functionality. Much like those previous studies conducted with skin derived LCs and DCs, internalisation of the fluorescent $PI_{C19\text{-}A3}$ AuNP complex by moDCs was both rapid and highly efficient (Figure 6A, B).

Investigating the interactions of AuNP-peptide treated MoDCs with T cells requires a T cell clone that is specific to the peptide. These clones were not available for $PI_{C19\text{-}A3}$ and so the GAD65 peptide ($GAD_{339\text{-}352}$) was used as a relevant autoantigen model, for which we had a $GAD_{339\text{-}352}$-specific memory T cell clone. To dissociate the influence of AuNPs on T cell stimulation from antigen uptake and processing, moDCs were incubated with AuNPs not coupled to an antigen (blank AuNPs) for 4 hours, at various concentrations (corresponding to 0.03, 0.3 and 3

μg/ml of gold), which were subsequently washed and incubated with either naïve allogeneic CD4+ T cells (Figure 7A) or a $GAD_{339-352}$-specific T cell clone in the presence of soluble $GAD_{339-352}$ peptide (Figure 7B). AuNPs reduced the capacity of DCs to stimulate proliferation of naive allo-reactive T cells in a dose dependent manner with respect to gold (Figure 7A), whilst a similar effect on GAD-specific memory T-cells was not apparent (Figure 7B). This suggests that AuNPs have a suppressive effect with respect to the presentation of a peptide to naïve T cells, which therefore prevents subsequent priming and activation. These findings agree with data showing that AuNPs, particularly smaller ones (10nm vs 50 nm), impair LPS-induced maturation and allo-stimulatory capacity of DCs(Tomic et al., 2014). This effect was not evident with memory T-cells, which may be explained by the fact that CD4 memory T-cells require less co-stimulation for activation in comparison to CD4+ naïve T cells. The impaired maturation of DCs may be valuable in promoting tolerance to antigen attached to AuNPs, for example in the treatment of autoimmunity, as immature DCs promote the generation of regulatory T cells(Suwandi et al., 2017).

To analyse the kinetics of antigen processing and presentation provided by the AuNP complexes, moDCs were pulsed with AuNPs coupled to $GAD_{339-352}$ peptide and incubated for 24-72 hours before used in a co-culture with the GAD-specific memory clone. Prolonged incubation of moDCs with AuNP $GAD_{339-352}$ complexes enhanced proliferation of GAD-specific effector T-cells compared to control moDCs that had been pulsed with soluble $GAD_{339-352}$ peptide alone (Figure 7C). This indicates that the peptide payload on AuNPs can be taken up, processed and presented efficiently by DCs to T cells, more efficiently than a soluble peptide, though in the context of this experiment the interaction was designed to give a stimulatory, rather than regulatory, effect.

4. CONCLUSIONS

This study has demonstrated and characterised localised delivery of self-peptide conjugated AuNPs into human skin via MicronJet600 hollow MNs. Adopting this delivery strategy supports three important pre-requisites for successful tolerance

induction through antigen specific immunotherapy, i.e. delivery (1) to the right tissue – the APC-rich epidermal layer of skin (2) to the right cells - predominantly LCs, and (3) in the right way - minimally invasive delivery with reduced DC activation (i.e. DCs remain in the immature state). Clinical studies are underway to determine if this system can indeed act as a platform for antigen specific tolerance induction.

5. FIGURES

Figure 1. A) Composition of AuNPs conjugated with $PI_{C19\text{-}A3}$ peptide, glutathione and either glucose (G) or mannose (M). B-D) TEM images of $PI_{C19\text{-}A3}$-AuNP complexes formulated with 5% glucose and different concentrations of the C19-A3 peptide (1% (B), 3% (C) or 10% (D). E, F) Stability of AuNP formulations both before and after injection through MicronJet600 MNs as measured by changes in E) particle size (nm) and zeta potential (mV) and F) gold concentration, as measured by UV/Vis absorbance.

Figure 2. Light microscopy images of control (A, D) and AuNPs injected (B, C, E, F) into fresh human skin using 600µm MicronJet MNs. Tissue biopsies were fixed at t=0h and t=4h and analysed for AuNP distribution. B, C) AuNPs formulated with 90%glutahthione/10%glucose were injected at concentration of 20 µg/ml (with respect to gold) and E) AuNPs containing 3% $PI_{C19\text{-}A3}$ peptide and 5%glucose were injected at concentration of 338 µg/ml (with respect to gold). F) Distribution of control 50nm AuNPs. SC = stratum corneum, E = epidermis, D = dermis.

Figure 3. TEM images of epidermal (A, B) and dermal cells (C) following injection of AuNPs (90%glutathione/10%glucose) (A) or a AuNP complex formulated with 1% of $PI_{C19\text{-}A3}$ peptide (B, C) using 600µm MicronJet MNs.

Figure 4. Flow cytometry of skin cells isolated from human skin 4 h after MJ600 injection of fluorescent 3%$PI_{C19\text{-}A3}$ AuNPs (corresponding to 300 µg/ml to gold). (A) Representative example of uptake by epidermal skin cells (expressed as MFI); (B) Representative example of uptake by dermal skins cells (expressed as MFI); (C) Percentage of FITC+ cells before (circles) and 4 h after (squares) FITC-labelled $PI_{C19\text{-}A3}$ AuNP injection into the human skin explants (n=4), note: uptake of HLA-DR+, CD11c- population was low i.e. <10% (data not shown). eDCs – epidermal DCs HLA-DR+, CD207+; other epidermal cells - HLA-DR-, CD207-; dDCs - dermal DCs HLA-DR+, CD11c+; other dermal cells HLA-DR-, CD11c-; solid grey – untreated; black line - after 4 h.

Figure 5. Internalisation of FITC-labelled $PI_{C19\text{-}A3}$ AuNPs into epidermal (A) and dermal (B) cells, isolated from skin explants, was confirmed using confocal microscopy. Injection concentration was 444 µg/ml (with respect to gold) corresponding to 10 µg of $PI_{C19\text{-}A3}$ in 50 µl water. Cells were stained with Hoescht (blue, nuclear staining), cell mask (red), FITC-labelled peptide (green).

Figure 6. Immature moDCs were incubated with PI_{C19A3} AuNPs (formulated with 3% peptide, 5% glucose). Fluorescence from released peptide was detected at 4 h using microscopy (A) and quantified using flow cytometry (B). Solid light grey – baseline; solid dark grey – after 4 h; dashed line - unstained.

Figure 7. Immature moDCs were incubated with AuNPs (no antigen, 5% glucose) at different concentrations (with respect to gold) for 4 h, and subsequently co-cultured with polyclonal naïve CD4+ T cells (A) or $GAD_{339-352}$-specific memory T cells in the presence of 5µg/ml soluble $GAD_{339-352}$ peptide (B). Proliferation (3H–thymidine incorporation) was measured after 3-days of co-culture. (A) AuNPs reduced the capacity of DCs to stimulate proliferation of naive alloreactive T cells. (B) AuNPs did not reduce the capacity of DCs to stimulate a GAD-specific T cell clone. (C) Immature moDCs were treated for 4h with soluble $GAD_{339-352}$ peptide (5µg/ml) or with AuNPs (3% $GAD_{339-352}$, 5% glucose, 27.5µg/ml gold) at a concentration corresponding to 5µg/ml GAD-peptide, and subsequently incubated with LPS (100ng/ml) for 24, 48 or 72 h. Thereafter DCs were collected, remaining free peptide or AuNPs was removed and DCs were co-cultured with $GAD_{339-352}$-specific memory T cells. Empty squares depict proliferation (3H–thymidine incorporation) of the GAD-clone when stimulated with soluble-peptide pulsed moDC. Dark squares depict proliferation when stimulated with AuNPs (loaded with peptide) pulsed moDC. Data show a representative of three independent moDC donors and was performed in triplicate.

Supplementary Figure 1. A) The NanoPass MicronJet600 device, consisting of three MNs, each 600µm in length and B) electron microscopy of a single NanoPass MN (enlarged by x330).

Supplementary Figure 2. Zeta potential distribution profiles of AuNP formulated with 1% of PI_{C19-A3} peptide (A, B) or 10% of PI_{C19-A3} peptide (C, D) before (A, C) and after (B, D) injection through 600µm MicronJet MNs.

Supplementary Figure 3. A) Flow cytometry data on cellular uptake of FITC-labelled AuNPs containing 3% PI_{C19A3}, 5%G in cultured HaCaT cells, primary human keratinocytes or in epidermal and dermal cells freshly isolated from human skin. B, C, D, E) Confocal microscopy images of the internalization of 3% PI_{C19A3} FITC-labelled AuNPs into HaCaTs (B), primary keratinocytes (C), epidermal (D) and dermal (E) cells isolated from excised human skin. Cells were stained with Hoescht (blue, nuclear staining), cell mask (red in B, C) and dendritic cell marker CD11c (red in E). FITC-labelled peptide is indicated in green.

Supplementary Movie 1. Internalisation of FITC-labelled PI_{C19-A3} AuNPs into primary keratinocytes following 4 h incubation with 3%PI_{C19-A3} 5%G. Cells were stained with Hoescht (blue, nuclear staining), cell mask (red), FITC-labelled peptide (green).

6. ACKNOWLEDGEMENTS

This work has been funded through the EE-ASI (The Enhanced Epidermal Antigen Specific Immunotherapy Against Type 1 Diabetes) European research network (Collaborative Project) supported by the European Commission under the Health Cooperation Work Programme of the 7th Framework Programme (Grant agreement N 305305).

The authors acknowledge the assistance and expertise of Christopher Von Ruhland with microscopy studies.

7. REFERENCES

Alhadj Ali, M., Liu, Y.F., Arif, S., Tatovic, D., Shariff, H., Gibson, V.B., Yusuf, N., Baptista, R., Eichmann, M., Petrov, N., Heck, S., Yang, J.H.M., Tree, T.I.M., Pujol-Autonell, I., Yeo, L., Baumard, L.R., Stenson, R., Howell, A., Clark, A., Boult, Z., Powrie, J., Adams, L., Wong, F.S., Luzio, S., Dunseath, G., Green, K., O'Keefe, A., Bayly, G., Thorogood, N., Andrews, R., Leech, N., Joseph, F., Nair, S., Seal, S., Cheung, H., Beam, C., Hills, R., Peakman, M., Dayan, C.M., 2017. Metabolic and immune effects of immunotherapy with proinsulin peptide in human new-onset type 1 diabetes. Science translational medicine 9 (402).

Anand, A., Zaman, K., Estivariz, C.F., Yunus, M., Gary, H.E., Weldon, W.C., Bari, T.I., Steven Oberste, M., Wassilak, S.G., Luby, S.P., Heffelfinger, J.D., Pallansch, M.A., 2015. Early priming with inactivated poliovirus vaccine (IPV) and intradermal fractional dose IPV administered by a microneedle device: A randomized controlled trial. Vaccine 33, 6816-6822.

Banchereau, J., Steinman, R.M., 1998. Dendritic cells and the control of immunity. Nature 392, 245-252.

Beals, C.R., Railkar, R.A., Schaeffer, A.K., Levin, Y., Kochba, E., Meyer, B.K., Evans, R.K., Sheldon, E.A., Lasseter, K., Lang, N., Weinberg, A., Canniff, J., Levin, M.J., 2016. Immune response and reactogenicity of intradermal administration versus subcutaneous administration of varicella-zoster virus vaccine: an exploratory, randomised, partly blinded trial. The Lancet. Infectious diseases 16, 915-922.

Boukamp, P., Petrussevska, R.T., Breitkreutz, D., Hornung, J., Markham, A., Fusenig, N.E., 1988. Normal keratinization in a spontaneously immortalized aneuploid human keratinocyte cell line. The Journal of cell biology 106, 761-771.

Bragazzi, N.L., Orsi, A., Ansaldi, F., Gasparini, R., Icardi, G., 2016. Fluzone(R) intra-dermal (Intanza(R)/Istivac(R) Intra-dermal): An updated overview. Human vaccines & immunotherapeutics 12, 2616-2627.

Coulman, S., Allender, C., Birchall, J., 2006. Microneedles and other physical methods for overcoming the stratum corneum barrier for cutaneous gene therapy. Critical reviews in therapeutic drug carrier systems 23, 205-258.

Coulman, S.A., Anstey, A., Gateley, C., Morrissey, A., McLoughlin, P., Allender, C., Birchall, J.C., 2009. Microneedle mediated delivery of nanoparticles into human skin. International journal of pharmaceutics 366, 190-200.

de Araujo, R.F.J., de Araujo, A.A., Pessoa, J.B., Freire Neto, F.P., da Silva, G.R., Leitao Oliveira, A.L., de Carvalho, T.G., Silva, H.F., Eugenio, M., Sant'Anna, C., Gasparotto, L.H., 2017. Anti-inflammatory, analgesic and anti-tumor properties of gold nanoparticles. Pharmacological reports : PR 69, 119-129.

Deckers, J., Hammad, H., Hoste, E., 2018. Langerhans Cells: Sensing the Environment in Health and Disease. Frontiers in immunology 9, 93.

Della Cioppa, G., Nicolay, U., Lindert, K., Leroux-Roels, G., Clement, F., Castellino, F., Galli, C., Groth, N., Levin, Y., Del Giudice, G., 2014. A dose-ranging study in older adults to compare the safety and immunogenicity profiles of MF59(R)-adjuvanted and non-adjuvanted seasonal influenza vaccines following intradermal and intramuscular administration. Human vaccines & immunotherapeutics 10, 1701-1710.

Edens, C., Collins, M.L., Goodson, J.L., Rota, P.A., Prausnitz, M.R., 2015a. A microneedle patch containing measles vaccine is immunogenic in non-human primates. Vaccine 33, 4712-4718.
Edens, C., Dybdahl-Sissoko, N.C., Weldon, W.C., Oberste, M.S., Prausnitz, M.R., 2015b. Inactivated polio vaccination using a microneedle patch is immunogenic in the rhesus macaque. Vaccine 33, 4683-4690.
Fernandez, T.D., Pearson, J.R., Leal, M.P., Torres, M.J., Blanca, M., Mayorga, C., Le Guevel, X., 2015. Intracellular accumulation and immunological properties of fluorescent gold nanoclusters in human dendritic cells. Biomaterials 43, 1-12.
Ghosh, P., Han, G., De, M., Kim, C.K., Rotello, V.M., 2008. Gold nanoparticles in delivery applications. Advanced drug delivery reviews 60, 1307-1315.
Henri, S., Guilliams, M., Poulin, L.F., Tamoutounour, S., Ardouin, L., Dalod, M., Malissen, B., 2010. Disentangling the complexity of the skin dendritic cell network. Immunology and cell biology 88, 366-375.
Hirsch, D.L., Ponda, P., 2015. Antigen-based immunotherapy for autoimmune disease: current status. ImmunoTargets and therapy 4, 1-11.
Hung, I.F., Levin, Y., To, K.K., 2012a. Quantitative and qualitative analysis of antibody response after dose sparing intradermal 2009 H1N1 vaccination. Vaccine 30, 2707-2708.
Hung, I.F., Levin, Y., To, K.K., Chan, K.H., Zhang, A.J., Li, P., Li, C., Xu, T., Wong, T.Y., Yuen, K.Y., 2012b. Dose sparing intradermal trivalent influenza (2010/2011) vaccination overcomes reduced immunogenicity of the 2009 H1N1 strain. Vaccine 30, 6427-6435.
Jones, D.P., Carlson, J.L., Samiec, P.S., Sternberg, P., Jr., Mody, V.C., Jr., Reed, R.L., Brown, L.A., 1998. Glutathione measurement in human plasma. Evaluation of sample collection, storage and derivatization conditions for analysis of dansyl derivatives by HPLC. Clinica chimica acta; international journal of clinical chemistry 275, 175-184.
Kang, B., Opatz, T., Landfester, K., Wurm, F.R., 2015. Carbohydrate nanocarriers in biomedical applications: functionalization and construction. Chemical Society reviews 44, 8301-8325.
Kim, J.H., Jang, H.H., Ryou, S.M., Kim, S., Bae, J., Lee, K., Han, M.S., 2010. A functionalized gold nanoparticles-assisted universal carrier for antisense DNA. Chemical communications 46, 4151-4153.
Kleijwegt, F.S., Laban, S., Duinkerken, G., Joosten, A.M., Zaldumbide, A., Nikolic, T., Roep, B.O., 2010. Critical role for TNF in the induction of human antigen-specific regulatory T cells by tolerogenic dendritic cells. Journal of immunology 185, 1412-1418.
Kochba, E., Levin, Y., Raz, I., Cahn, A., 2016. Improved Insulin Pharmacokinetics Using a Novel Microneedle Device for Intradermal Delivery in Patients with Type 2 Diabetes. Diabetes technology & therapeutics 18, 525-531.
Kohli, A.K., Alpar, H.O., 2004. Potential use of nanoparticles for transcutaneous vaccine delivery: effect of particle size and charge. International journal of pharmaceutics 275, 13-17.
Labouta, H.I., el-Khordagui, L.K., Kraus, T., Schneider, M., 2011. Mechanism and determinants of nanoparticle penetration through human skin. Nanoscale 3, 4989-4999.

Levin, Y., Kochba, E., Hung, I., Kenney, R., 2015. Intradermal vaccination using the novel microneedle device MicronJet600: Past, present, and future. Human vaccines & immunotherapeutics 11, 991-997.
Levin, Y., Kochba, E., Kenney, R., 2014. Clinical evaluation of a novel microneedle device for intradermal delivery of an influenza vaccine: are all delivery methods the same? Vaccine 32, 4249-4252.
Levin, Y., Kochba, E., Shukarev, G., Rusch, S., Herrera-Taracena, G., van Damme, P., 2016. A phase 1, open-label, randomized study to compare the immunogenicity and safety of different administration routes and doses of virosomal influenza vaccine in elderly. Vaccine 34, 5262-5272.
Loumaigne, M., Praho, R., Nutarelli, D., Werts, M.H., Debarre, A., 2010. Fluorescence correlation spectroscopy reveals strong fluorescence quenching of FITC adducts on PEGylated gold nanoparticles in water and the presence of fluorescent aggregates of desorbed thiolate ligands. Physical chemistry chemical physics : PCCP 12, 11004-11014.
Love, J.C., Estroff, L.A., Kriebel, J.K., Nuzzo, R.G., Whitesides, G.M., 2005. Self-assembled monolayers of thiolates on metals as a form of nanotechnology. Chemical reviews 105, 1103-1169.
Mansoor, I., Lai, J., Ranamukhaarachchi, S., Schmitt, V., Lambert, D., Dutz, J., Hafeli, U.O., Stoeber, B., 2015. A microneedle-based method for the characterization of diffusion in skin tissue using doxorubicin as a model drug. Biomedical microdevices 17, 9967.
McAllister, D.V., Wang, P.M., Davis, S.P., Park, J.H., Canatella, P.J., Allen, M.G., Prausnitz, M.R., 2003. Microfabricated needles for transdermal delivery of macromolecules and nanoparticles: fabrication methods and transport studies. Proceedings of the National Academy of Sciences of the United States of America 100, 13755-13760.
Merad, M., Ginhoux, F., Collin, M., 2008. Origin, homeostasis and function of Langerhans cells and other langerin-expressing dendritic cells. Nature reviews. Immunology 8, 935-947.
Mutyambizi, K., Berger, C.L., Edelson, R.L., 2009. The balance between immunity and tolerance: the role of Langerhans cells. Cellular and molecular life sciences : CMLS 66, 831-840.
Pearton, M., Pirri, D., Kang, S.M., Compans, R.W., Birchall, J.C., 2013. Host responses in human skin after conventional intradermal injection or microneedle administration of virus-like-particle influenza vaccine. Advanced healthcare materials 2, 1401-1410.
Prausnitz, M.R., 2017. Engineering Microneedle Patches for Vaccination and Drug Delivery to Skin. Annual review of chemical and biomolecular engineering 8, 177-200.
Rana, S., Bajaj, A., Mout, R., Rotello, V.M., 2012. Monolayer coated gold nanoparticles for delivery applications. Advanced drug delivery reviews 64, 200-216.
Schloot, N.C., Batstra, M.C., Duinkerken, G., De Vries, R.R., Dyrberg, T., Chaudhuri, A., Behan, P.O., Roep, B.O., 1999. GAD65-Reactive T cells in a non-diabetic stiff-man syndrome patient. Journal of autoimmunity 12, 289-296.
Sies, H., 1999. Glutathione and its role in cellular functions. Free radical biology & medicine 27, 916-921.
Sonavane, G., Tomoda, K., Sano, A., Ohshima, H., Terada, H., Makino, K., 2008. In vitro permeation of gold nanoparticles through rat skin and rat intestine: effect of particle size. Colloids and surfaces. B, Biointerfaces 65, 1-10.

Suwandi, J.S., Nikolic, T., Roep, B.O., 2017. Translating Mechanism of Regulatory Action of Tolerogenic Dendritic Cells to Monitoring Endpoints in Clinical Trials. Frontiers in immunology 8, 1598.
Thrower, S.L., James, L., Hall, W., Green, K.M., Arif, S., Allen, J.S., Van-Krinks, C., Lozanoska-Ochser, B., Marquesini, L., Brown, S., Wong, F.S., Dayan, C.M., Peakman, M., 2009. Proinsulin peptide immunotherapy in type 1 diabetes: report of a first-in-man Phase I safety study. Clinical and experimental immunology 155, 156-165.
Tomic, S., Ethokic, J., Vasilijic, S., Ogrinc, N., Rudolf, R., Pelicon, P., Vucevic, D., Milosavljevic, P., Jankovic, S., Anzel, I., Rajkovic, J., Rupnik, M.S., Friedrich, B., Colic, M., 2014. Size-dependent effects of gold nanoparticles uptake on maturation and antitumor functions of human dendritic cells in vitro. PloS one 9, e96584.
Troy, S.B., Kouiavskaia, D., Siik, J., Kochba, E., Beydoun, H., Mirochnitchenko, O., Levin, Y., Khardori, N., Chumakov, K., Maldonado, Y., 2015. Comparison of the Immunogenicity of Various Booster Doses of Inactivated Polio Vaccine Delivered Intradermally Versus Intramuscularly to HIV-Infected Adults. The Journal of infectious diseases 211, 1969-1976.
Van Damme, P., Oosterhuis-Kafeja, F., Van der Wielen, M., Almagor, Y., Sharon, O., Levin, Y., 2009. Safety and efficacy of a novel microneedle device for dose sparing intradermal influenza vaccination in healthy adults. Vaccine 27, 454-459.
von Herrath, M., Peakman, M., Roep, B., 2013. Progress in immune-based therapies for type 1 diabetes. Clinical and experimental immunology 172, 186-202.
Zhao, X., Birchall, J.C., Coulman, S.A., Tatovic, D., Singh, R.K., Wen, L., Susan Wong, F., Dayan, C.M., Hanna, S.J., 2016. Microneedle delivery of autoantigen for immunotherapy in type 1 diabetes. Journal of controlled release : official journal of the Controlled Release Society 223, 178-187.

*Graphical Abstract (for review)

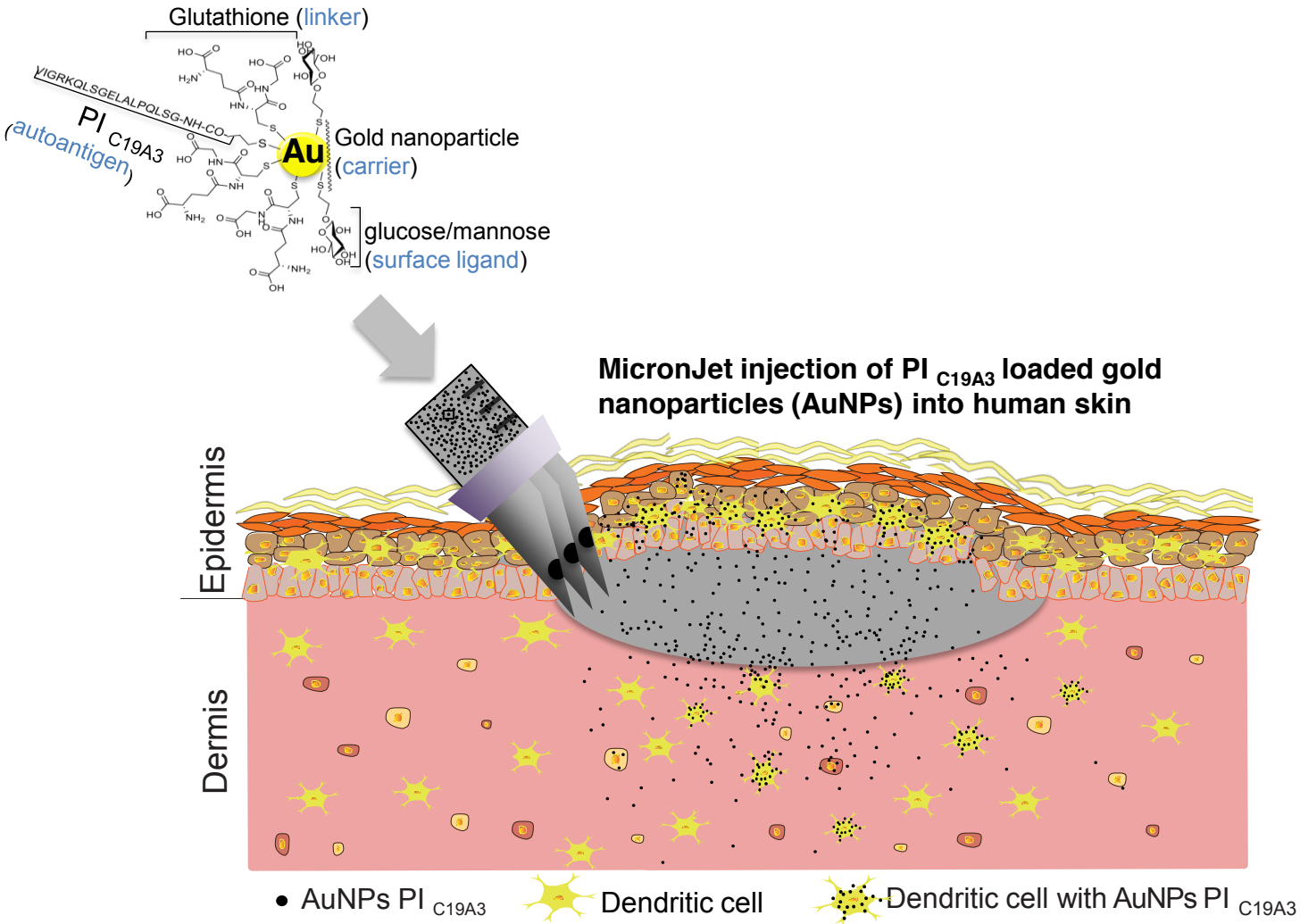

Figure 1

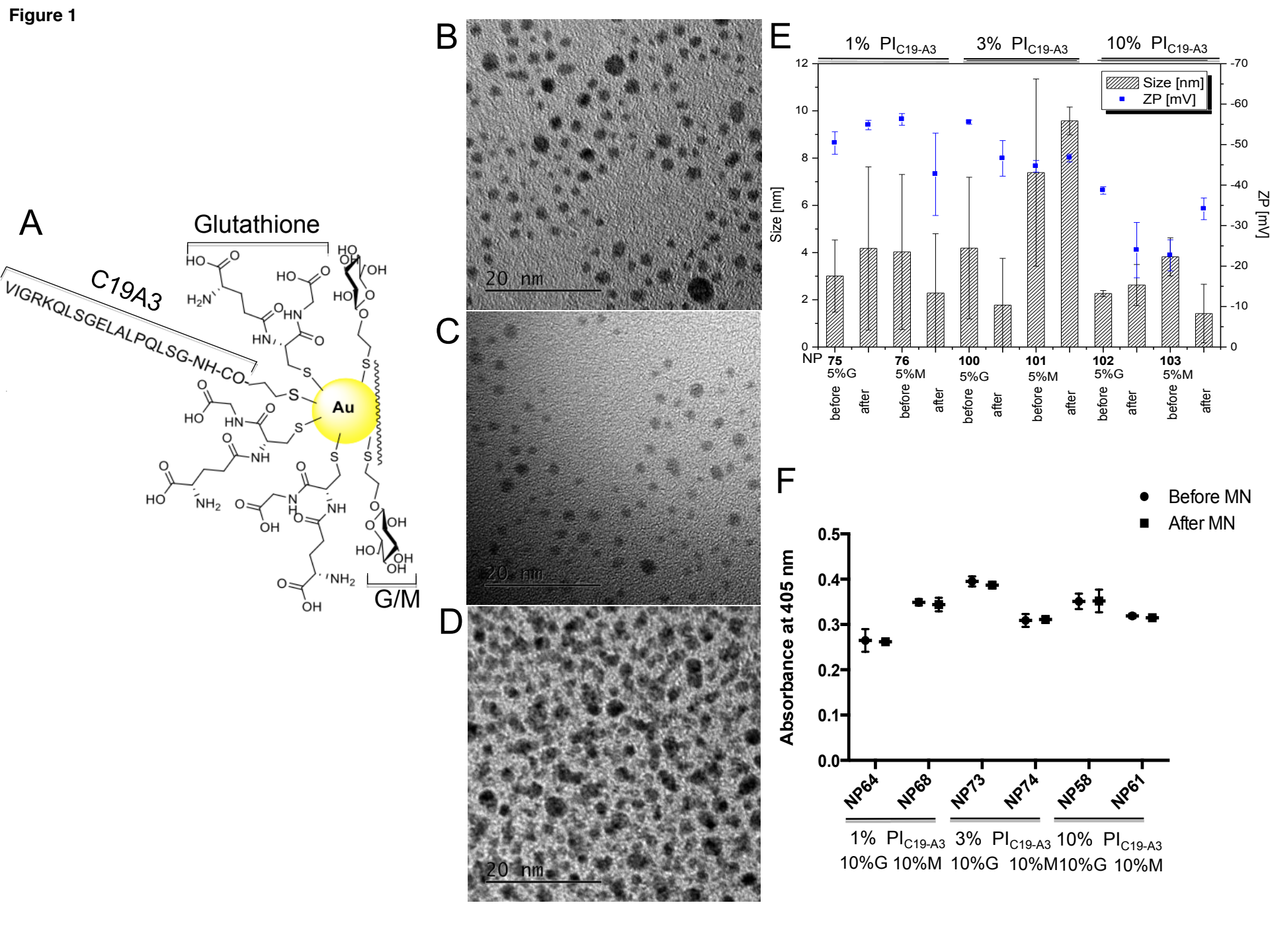
A
Glutathione
C19A3
VIGRKQLSGELALPQLSG-NH-CO
Au
G/M
B
20 nm
C
20 nm
D
20 nm
E
1% PIC19-A3
3% PIC19-A3
10% PIC19-A3
Size [nm]
ZP [mV]
NP
75 5%G
76 5%M
100 5%G
101 5%M
102 5%G
103 5%M
before
after
F
Before MN
After MN
Absorbance at 405 nm
NP64
NP68
NP73
NP74
NP58
NP61
1% PIC19-A3 10%G 10%M
3% PIC19-A3 10%G 10%M
10% PIC19-A3 10%G 10%M

Figure 2

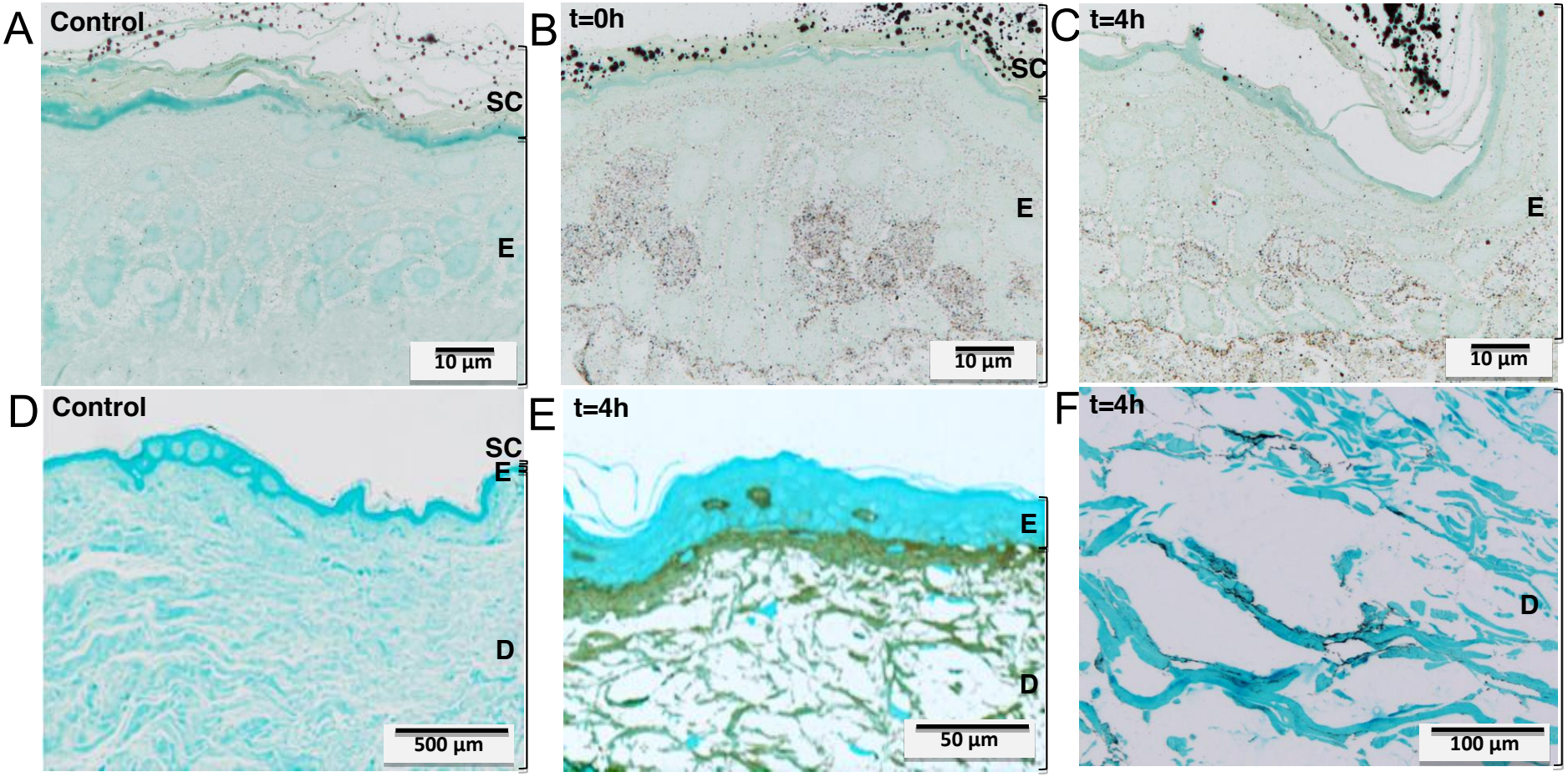
A
Control
SC
E
10 µm
B
t=0h
SC
E
10 µm
C
t=4h
E
10 µm
D
Control
SC
E
D
500 µm
E
t=4h
E
D
50 µm
F
t=4h
D
100 µm

Figure 3

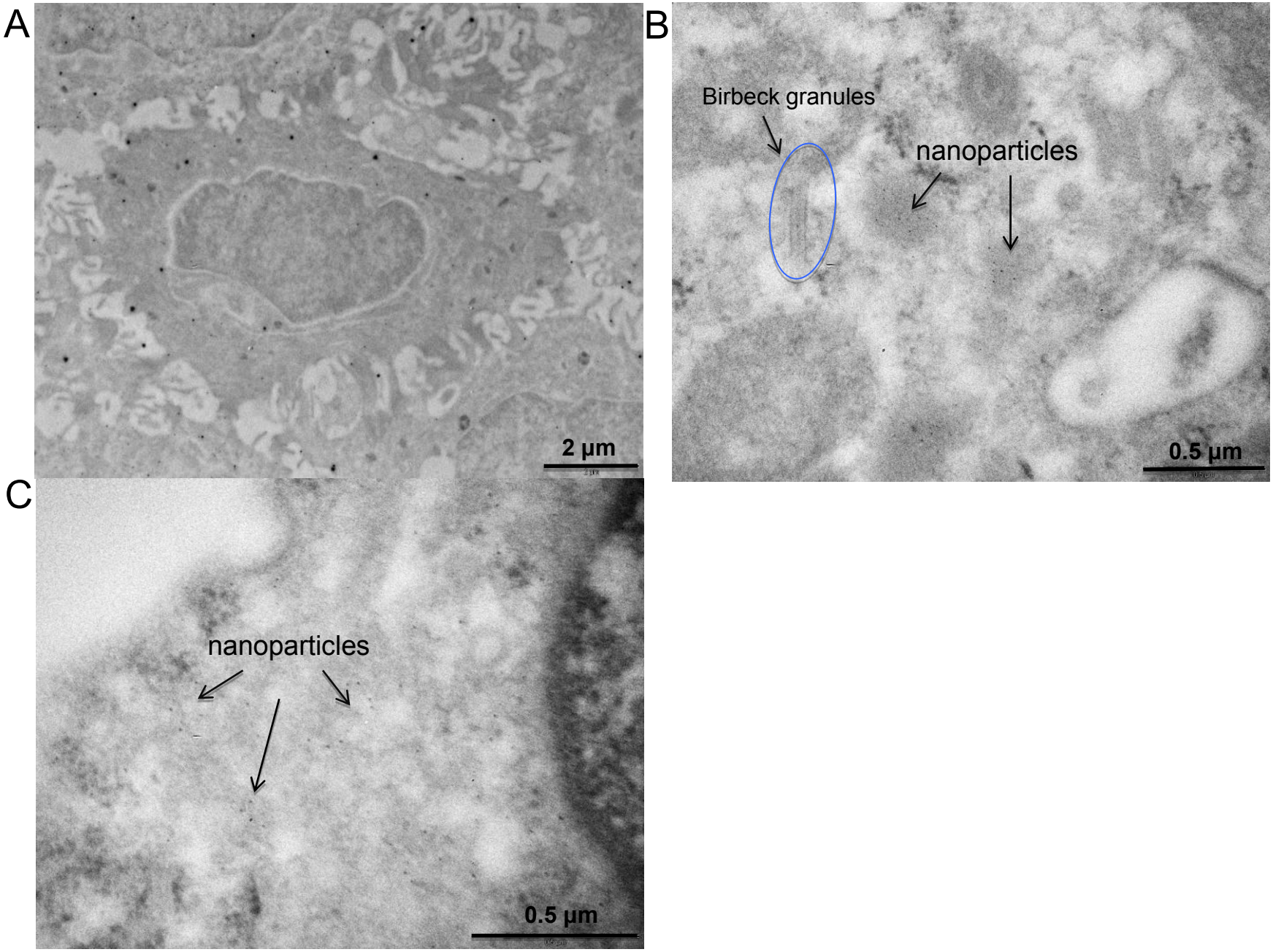
A
2 µm
B
Birbeck granules
nanoparticles
0.5 µm
C
nanoparticles
0.5 µm

Figure 4

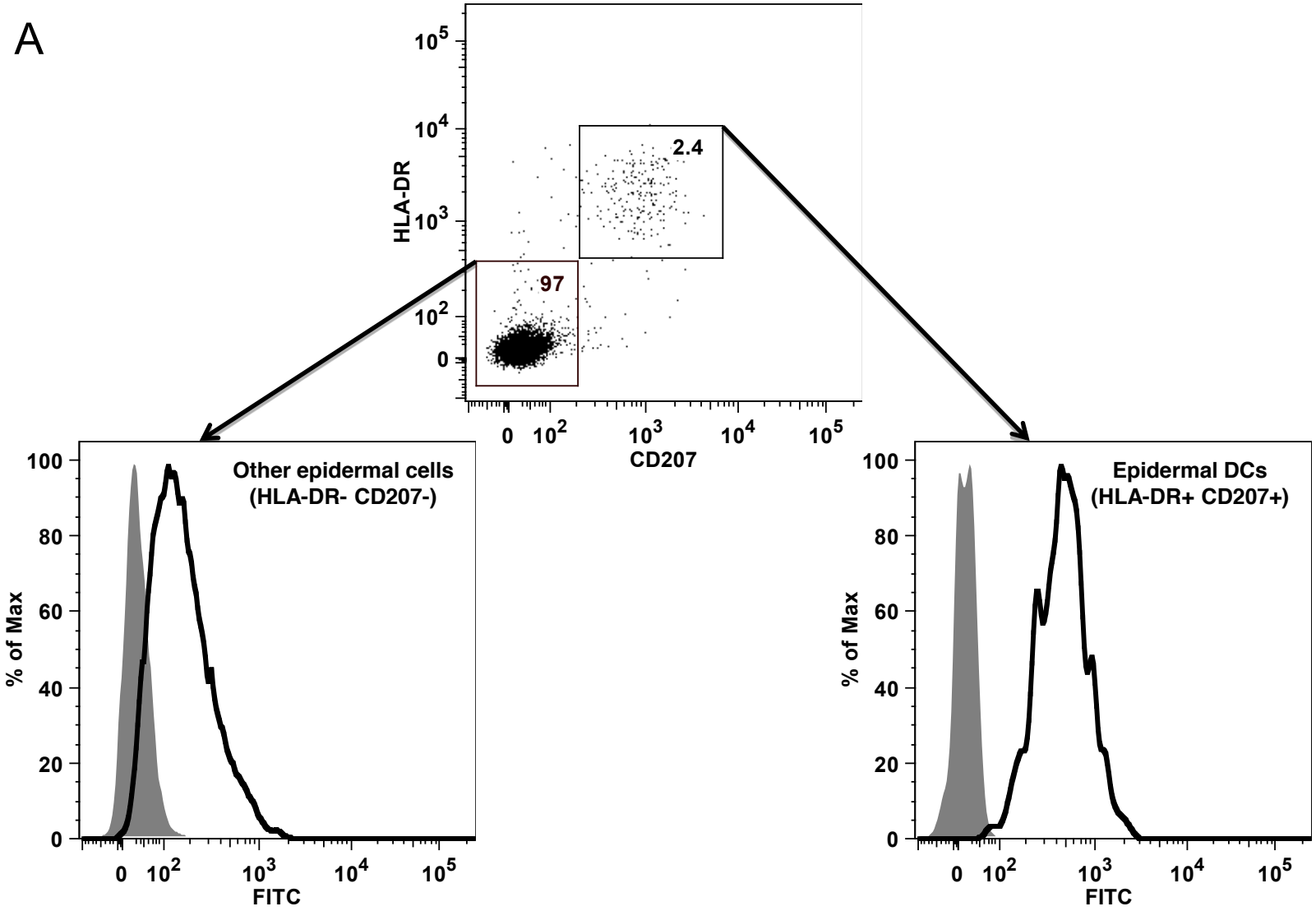
A
HLA-DR
CD207
2.4
97
Other epidermal cells
(HLA-DR- CD207-)
Epidermal DCs
(HLA-DR+ CD207+)
% of Max
FITC

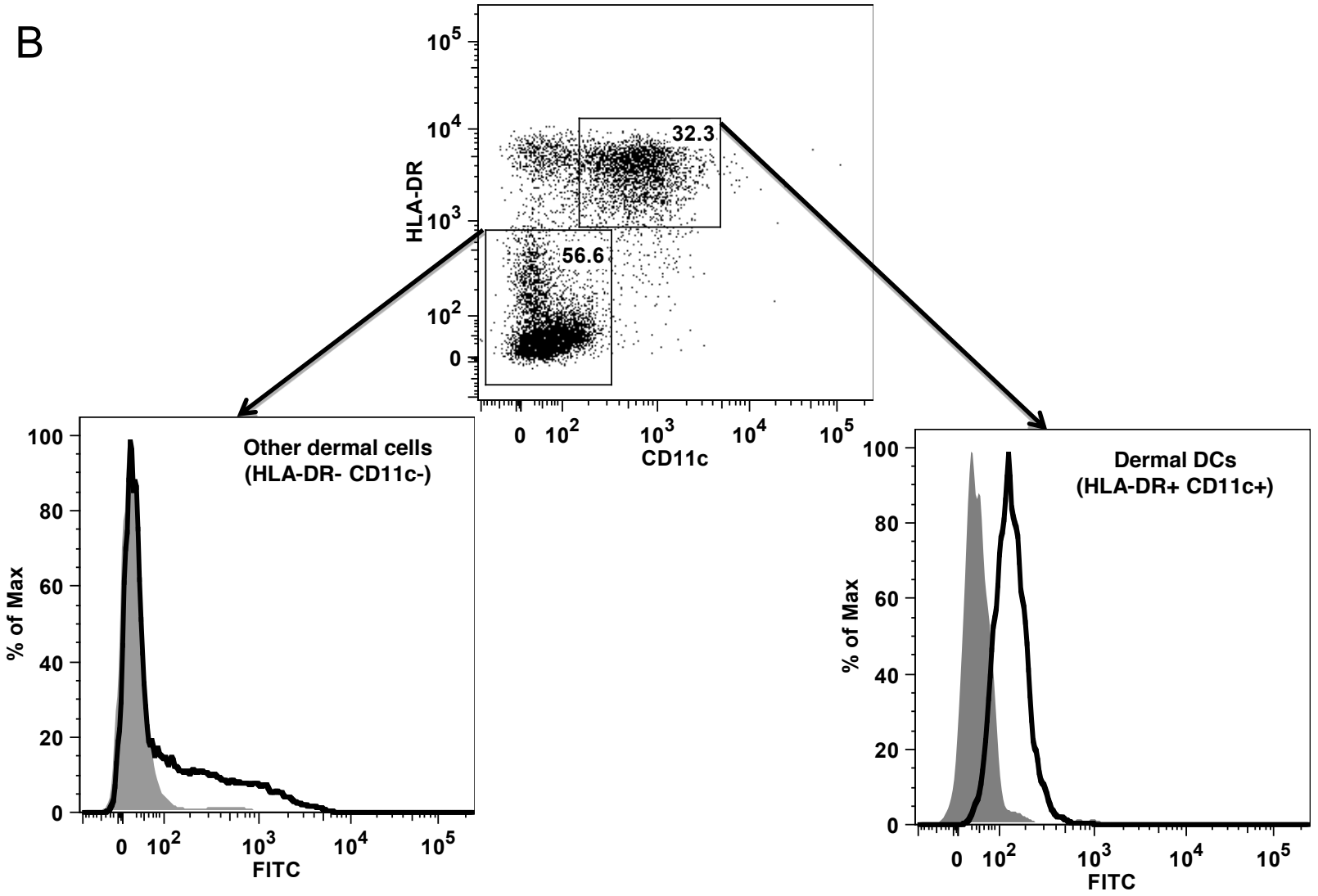
B
HLA-DR
CD11c
32.3
56.6
Other dermal cells
(HLA-DR- CD11c-)
Dermal DCs
(HLA-DR+ CD11c+)
% of Max
FITC

C

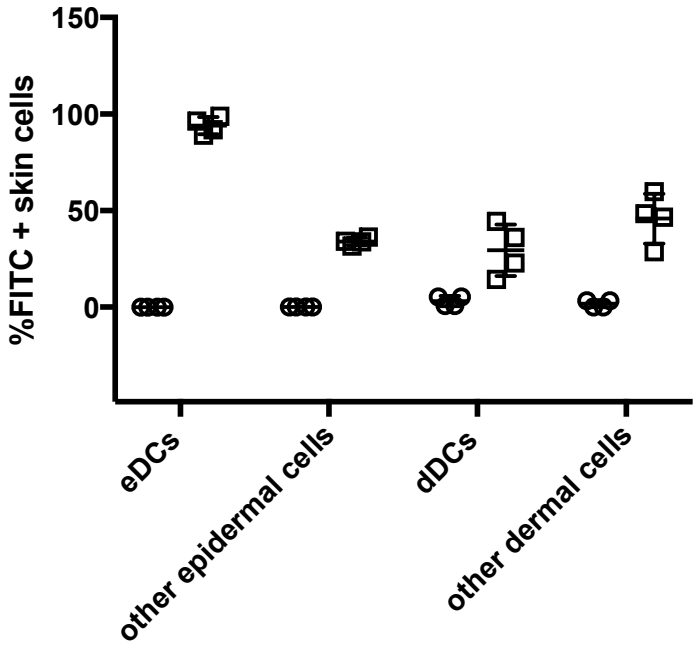
150
100
50
0
%FITC + skin cells
eDCs
other epidermal cells
dDCs
other dermal cells

Figure 5

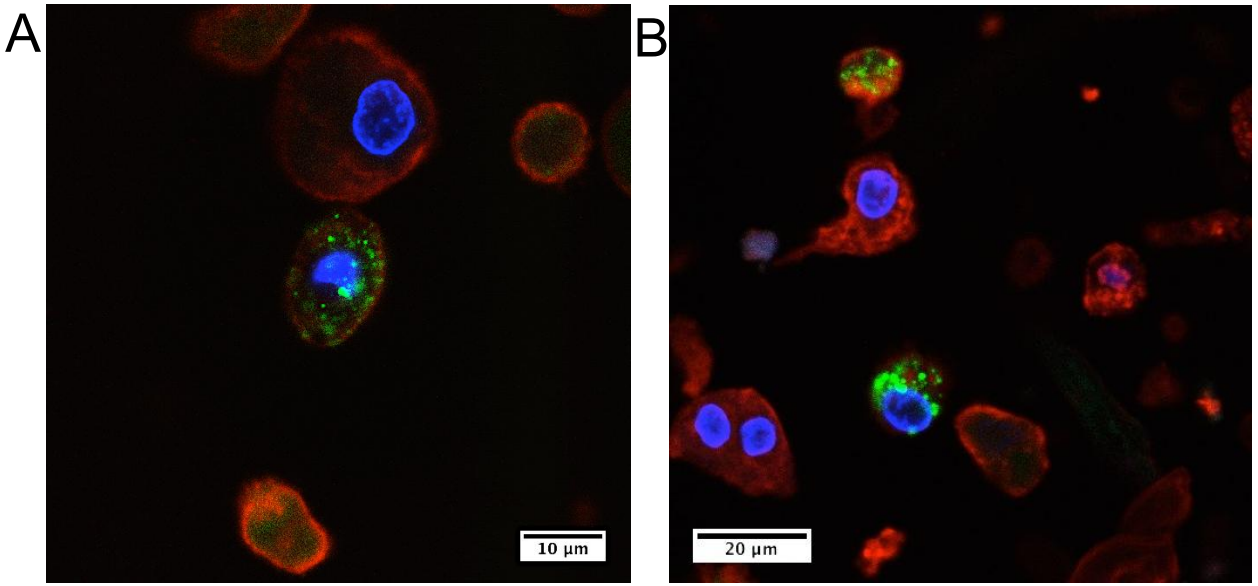

Figure 6

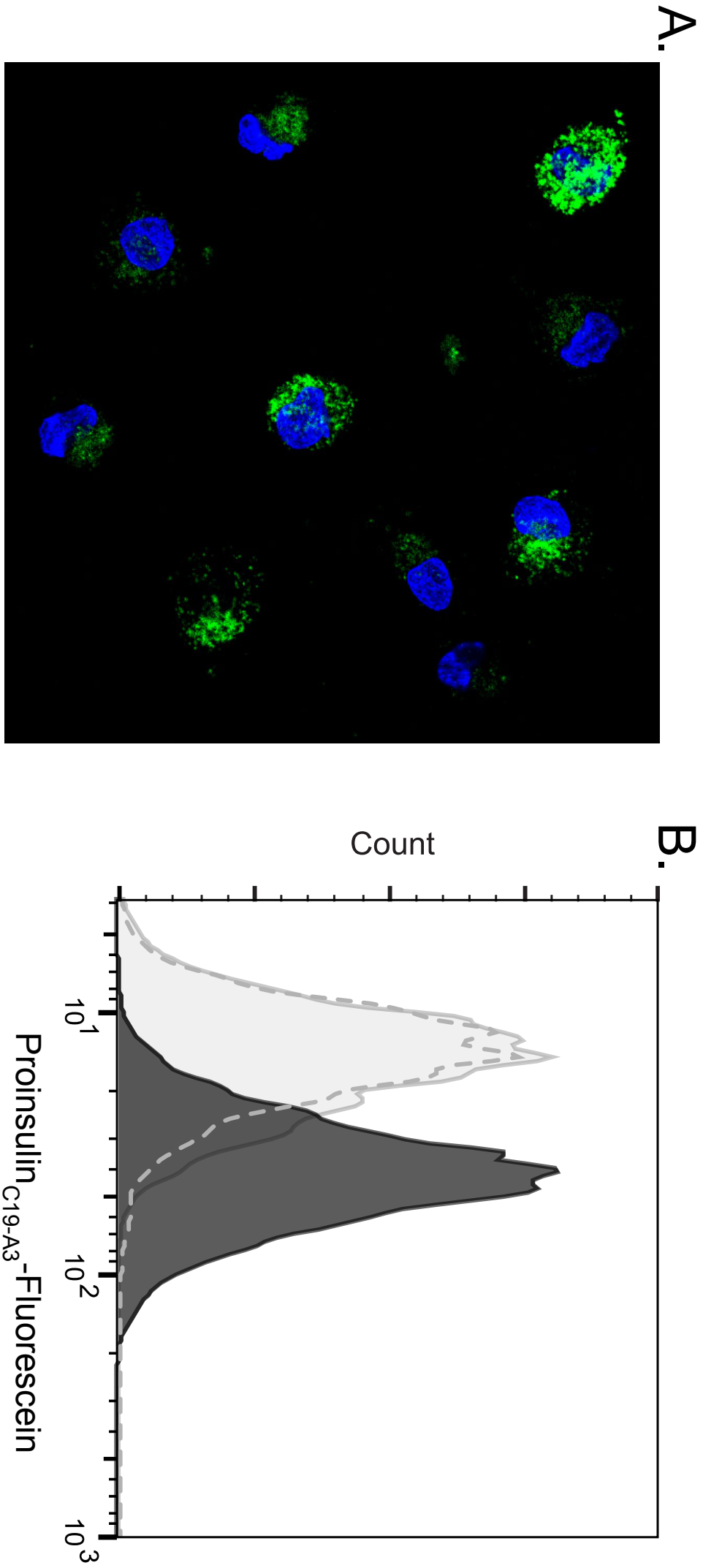

Figure 7

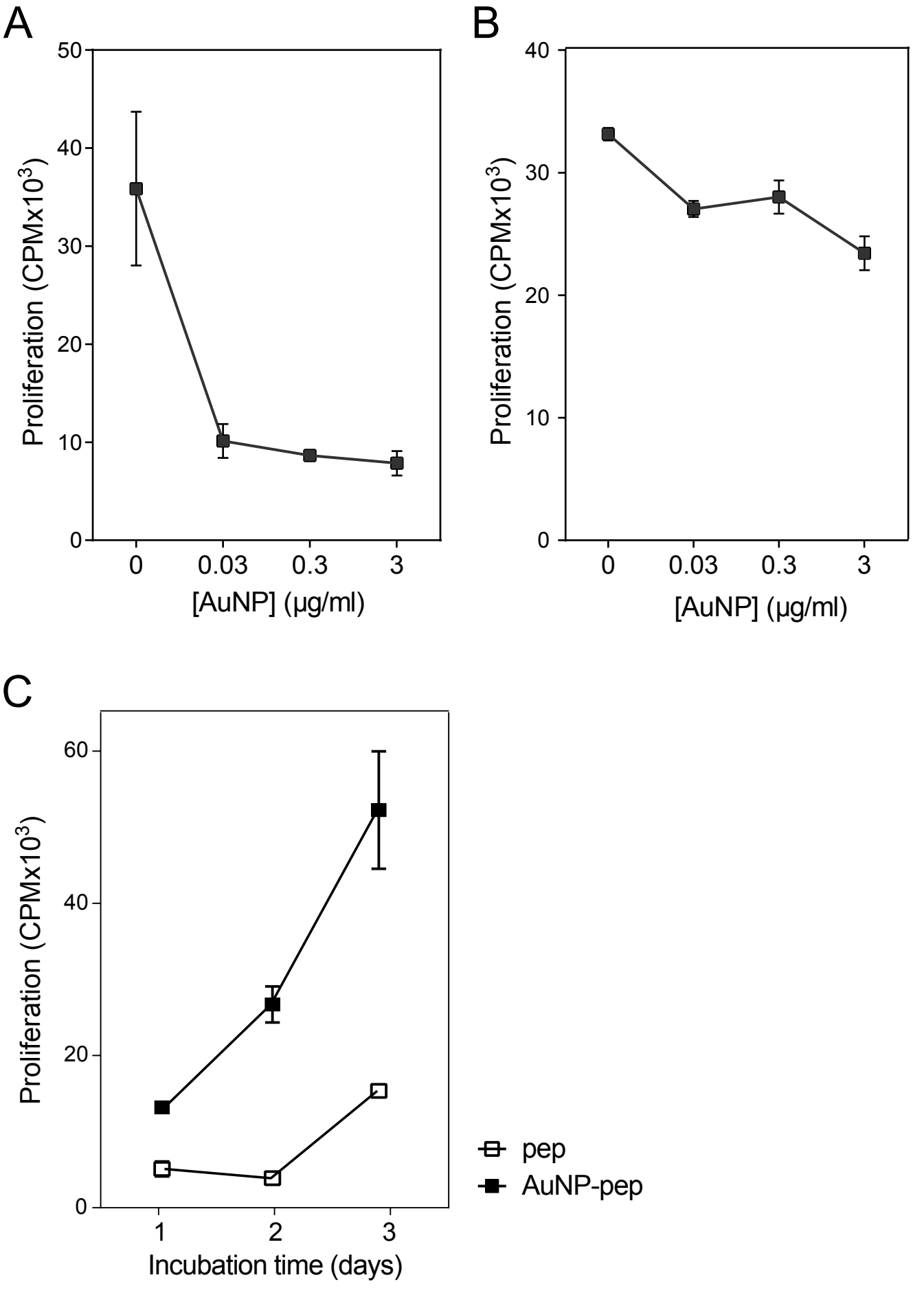
A
Proliferation (CPMx10^3)
50
40
30
20
10
0
0
0.03
0.3
3
[AuNP] (µg/ml)
B
Proliferation (CPMx10^3)
40
30
20
10
0
0
0.03
0.3
3
[AuNP] (µg/ml)
C
Proliferation (CPMx10^3)
60
40
20
0
1
2
3
Incubation time (days)
pep
AuNP-pep

Supplementary Figure 1

Click here to download Supplementary Material: Suppl Figure 1 0512.tif

Supplementary Figure 2

Click here to download Supplementary Material: Suppl Figure 2 0512.jpg

Supplementary Figure 3

Click here to download Supplementary Material: Suppl Figure 3 0512.ppt

Movie

Click here to download Supplementary Material: Movie.avi

***Conflict of Interest**

Declaration of interests

☐ The authors declare that they have no known competing financial interests or personal relationships that could have appeared to influence the work reported in this paper.

☐The authors declare the following financial interests/personal relationships which may be considered as potential competing interests:

Patent 'Nanoparticle-based antigen specific immunotherapy' was filed on 10th April 2015, Application number GB 1506112.0.

Yotam Levin is CEO of NanoPass Technologies Ltd. Efrat Kochba is the Medical Director of Nanopass Technologies Ltd.